

Facile Preparation and Highly Efficient Sorption of Magnetic Composite Graphene Oxide/Fe₃O₄/GC for Uranium Removal

Aili Yang (✉ yang770117@sina.com)

China Academy of Engineering Physics

Zhijun Wang

China Academy of Engineering Physics

Yukuan Zhu

China Academy of Engineering Physics

Research Article

Keywords: Graphene oxide, magnetic, thermodynamic

Posted Date: January 29th, 2021

DOI: <https://doi.org/10.21203/rs.3.rs-150676/v1>

License:  This work is licensed under a Creative Commons Attribution 4.0 International License.

[Read Full License](#)

Version of Record: A version of this preprint was published at Scientific Reports on April 19th, 2021. See the published version at <https://doi.org/10.1038/s41598-021-86768-0>.

Facile preparation and highly efficient sorption of magnetic composite graphene oxide/Fe₃O₄/GC for uranium removal

Aili Yang¹, Zhijun Wang¹ & Yukuan Zhu¹

In this work, we reported for the first time a novel magnetic composite graphene oxide/Fe₃O₄/glucose-COOH (GO/Fe₃O₄/GC) that was facilely prepared from glucose through the hydrothermal carbonization and further combination with graphene oxide (GO). The chemical and structural properties of the samples were investigated. By the batch uranium adsorption experiments, the magnetic composite GO/Fe₃O₄/GC exhibits an excellent adsorption performance and fast solid-liquid separation for uranium from aqueous solution. GO/Fe₃O₄/GC (the maximum adsorption capacity (Q_m) was 390.70 mg g⁻¹) exhibited excellent adsorption capacity and higher removal rate (> 99%) for U(VI) than those of glucose-COOH (GC) and magnetic GC (MGC). The effect of the coexisting ions, such as Na⁺, K⁺, Mg²⁺, Ca²⁺, and Al³⁺, on the U(VI) removal efficiency of GO/Fe₃O₄/GC was examined. The equilibrium sorption and sorption rate for the as-prepared adsorbents well fit the Langmuir model and pseudo second-order kinetic model, respectively. The thermodynamic parameters ($\Delta H^0 = 11.57 \text{ kJ mol}^{-1}$ and $\Delta G^0 < 0$) for GO/Fe₃O₄/GC indicate that the sorption process of U(VI) was exothermic and spontaneous. Thus, this research provides a facile strategy for the preparation of the magnetic composite with low cost, high efficiency and fast separation for the U(VI) removal from aqueous solution.

Nowadays, carbonaceous materials, such as activated carbon¹, carbon nanotubes², carbon fibre³, and mesoporous carbon⁴, have been widely applied due to their availability, acid-base stability, and thermal resistance. These carbonaceous materials generally are fabricated via high temperature reaction⁵, pyrolysis⁶⁻⁸, gasification⁹, electrospinning technique¹⁰, *etc.* Amongst these techniques, hydrothermal carbonization (HTC) has become a proficient synthesis technique owing to its cheapness, simplification, mild reaction conditions, and lack of any organic solvent and toxic waste. The fabrication of the biomass modification product by HTC process is one of the hot spots in recent years¹¹⁻¹³. As a branch of carbonaceous materials the HTC materials from biomass have emerged since 1913¹⁴, and exhibited significant potential in various fields, such as adsorption¹⁵⁻¹⁸, catalysis¹⁹, fuel cell²⁰, and energy storage/conversion²¹⁻²³. Among the potential precursors for the preparation of HTC materials, glucose as a promising candidate has drawn much attention²⁴. Glucose with low-cost and non-toxicity is a natural organic biomass, and reacts with heavy metals and influence their migration behaviour.

With increasing development of all kinds of industry, severe water pollution caused by reckless discharge into water has critically threatened human health and ecosystem²⁵. Adsorption is a popular technique to resolve water contamination problems due to its low energy consumption, easiness, effectiveness, and no secondary pollution^{26,27}. The glucose-based adsorbents have been proved to be promising for the removal of various pollutants, such as antibiotics²⁸, organic pollutants²⁹, gas pollutants³⁰, dyes³¹, and heavy metal ions^{32,33}. However, glucose treated solely by a hydrothermal approach possesses poor pore configuration, undeveloped porosity and low adsorption capacity, which make it being rarely applied in the removal of the pollutants¹². Therefore, it is significant to develop novel glucose derivatives with numerous functional group in order to enhance the property.

Graphene oxide (GO) has been proved a popular candidate as a template for fabricating other functional nanomaterials, owing to its unique layered structure and remarkable physicochemical properties, such as high surface area, hydrophobicity, conductivity, and elasticity. Moreover, GO as an adsorbent can efficiently capture contaminants in water for water remediation³⁴. However, the excellent dispersion of GO increases difficulty in separation between GO and treated solution, and tend to agglomerate after adsorption which lessens the adsorption capacity of GO³⁵. To overcome these drawbacks of GO, the functionalization of GO with other materials, such as glucose, has become a promising tendency³⁶. The addition of inexpensive glucose onto GO can effectively reduce the production cost of the adsorbent, and obtain abundant active

¹Aili Yang: Institute of Materials, China Academy of Engineering Physics, P.O. Box 9071-7, Mianyang, 621907, China.

²Zhijun Wang: Institute of Materials, China Academy of Engineering Physics, P.O. Box 9071-7, Mianyang, 621907, China.

³Yukuan Zhu: Institute of Materials, China Academy of Engineering Physics, P.O. Box 9071-7, Mianyang, 621907, China.

Correspondence and requests for materials should be addressed to Aili Yang. (Email: yang770117@sina.com, Tel/Fax: 086-18380598619/086-0816-3625900).

oxygen group simultaneously. Xie et al synthesized glucose-based carbon nanosheets by an integrated GO-confined nanospace directed KOH-activated process for the removal of sulfamethazine³⁷. Martín-Jimeno et al prepared HTC xerogels via hydrothermal carbonization of glucose in the presence of GO as morphology directing agent and KOH activation method for CO₂ and dye adsorption³⁸. However, the preparation methods for these glucose-based composites have some major drawbacks, such as high energy cost, operation complexity, and solid-liquid separation difficulty.

In order to overcome the separation problem, green and inexpensive magnetic nanoparticles, such as Fe₃O₄, have drawn considerable attention due to their environmentally friendliness and unique magnetic behaviour³⁹⁻⁴¹. The existence of Fe₃O₄ makes solid substance be rapidly separated from liquid phase only through an external magnetic field to shorten the wastewater treatment period. To our best knowledge, few researches focus on the preparation of the magnetic glucose-based adsorbent with GO as the template for the removal of uranium. Herein, in the present work, a magnetic GO-functionalized HTC adsorbent (GO/Fe₃O₄/GC) was synthesized using glucose as the carbon precursor via hydrothermal carbonization and magnetization reaction, which aims to develop a novel high-efficiency adsorbent for the removal of U(VI) from nuclear waste influent. The fabrication process and magnetization curve of GO/Fe₃O₄/GC (magnetization saturation value is 23.79 emu g⁻¹) are shown in Fig. 1. The samples were characterized by elements analysis, crystal phase, functional group, and thermal stability. To evaluate the removal performance of the samples for U(VI), the batch adsorption experiments were carried out, and the kinetic and thermodynamic parameters in the adsorption process were provided.

Results and discussion

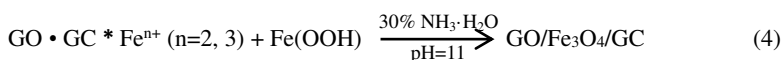
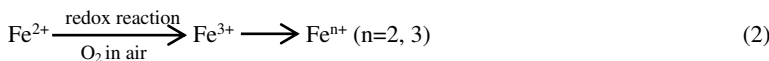
Characterization. The FTIR spectra of glucose, Fe₃O₄, GC, MGC and GO/Fe₃O₄/GC were shown in Fig. 2A. In the IR spectrum of GC, most of the characteristic peaks disappeared compared to glucose, but the intensity of the band at 1714 cm⁻¹ was higher than that of glucose, which indicated that GC was successfully obtained after hydrothermal and calcination treatment, and the number of carboxyl, carbonyl and ester groups significantly increased on the surface. These characteristic peaks of GC were similar to those of HTC-COOH reported in the reference [42]. In the IR spectrum of GO/Fe₃O₄/GC, the characteristic peaks at ~567 cm⁻¹ and ~352 cm⁻¹ belonged to Fe-O stretching vibration appeared, suggesting that the magnetic composite GO/Fe₃O₄/GC was successfully prepared.

The XRD crystal phases of the samples were presented in Fig. 2B. In the XRD pattern of glucose, the strong diffraction peaks reflected great crystallization of glucose. However, the crystal phase of GC is amorphous owing to the calcination process in 300 °C, which accords with the reference [43]. The structures of MGC and GO/Fe₃O₄/GC are also amorphous due to the existence of GC. Moreover, the XRD peaks at 2θ values of the purchased Fe₃O₄ are about 29.94°, 35.30°, 42.98°, 53.38°, 56.84°, 62.46° and 74.84°. The XRD patterns of GO/Fe₃O₄/GC and MGC are basically consistent with those of Fe₃O₄, while the intensity of the peaks has significantly reduced compared to Fe₃O₄ because of the addition of GO and GC.

To reveal the thermal stability of the samples, the TGA curves of glucose, GC, MGC and GO/Fe₃O₄/GC in the range of temperatures from 30 to 900 °C are shown in Fig. 2C. The composite GO/Fe₃O₄/GC presented the smallest weight loss (4.28%) when the temperature was up to 900 °C, which showed that GO/Fe₃O₄/GC had the excellent thermal stability and almost no thermal decomposition took place. While the thermal stability of glucose, GC and MGC was poor, and the weight losses at 900 °C were 76.79%, 49.67% and 16.48%, respectively.

The element composition of Fe₃O₄, glucose, GC, MGC and GO/Fe₃O₄/GC was investigated by XPS. The XPS survey spectrum of GO/Fe₃O₄/GC (Fig. 3A) shows that the evident characteristic peaks at about 285, 554, 711 and 725 eV attributed to C1s, O1s and Fe2p, respectively. In the high-resolution spectrum of Fe 2p (Fig. 3B), the peaks of Fe 2p_{3/2} and Fe 2p_{1/2} are located at 711.30 eV and 724.70 eV, respectively, indicating the presence of Fe₃O₄ in the composite GO/Fe₃O₄/GC.

Based on the above characterization results, a possible formation mechanism for GO/Fe₃O₄/GC is illustrated in Fig. 4. Firstly, GO nanosheet is physically mixed with GC in an ultrasonic bath to form the complex GO • GC through hydrogen bond interaction as shown in Eq. (1). Then, Feⁿ⁺ (n = 2, 3) ions were formed in the above suspension by adding Fe²⁺ ions because a part of Fe²⁺ ions were oxidized to Fe³⁺ in air by the redox reaction as shown in Eq. (2). With the hydrolysis of Fe³⁺ and the addition of 30% ammonia solution the magnetic composite GO/Fe₃O₄/GC was obtained as expressed in Eqs. (3) and Eq. (4). Thus, both GC and Fe₃O₄ are immobilized on the surface of GO.



Adsorption tests. The effect of the solution pH on the adsorption efficiency of the as-prepared adsorbents toward U(VI) is exhibited in Fig. 5A. The results show that the adsorption process for U(VI) obviously depends on the pH value of the solution. The pH value of the solutions greatly affects the surface charge of the samples. At pH < 4.0, the surface of the sorbents were protonated to form the positively charged surface, and then the electrostatic repulsion between these positive charge (including H_3O^+) and UO_2^{2+} led to the poor adsorption capability for U(VI).¹⁴ With the appearance of the positive species ($\text{UO}_2(\text{OH})^+$, $(\text{UO}_2)_3(\text{OH})_5^+$, and $(\text{UO}_2)_4(\text{OH})_7^+$) the removal efficiency of U(VI) significantly increased at pH 4.0–7.0 due to the electrostatic interaction between these complex uranium ions with positive charges and the negatively charged adsorbents. When pH is above 7.0, the negatively charged U(VI) species ($(\text{UO}_2)_3(\text{OH})_7^-$ and $\text{UO}_2(\text{OH})_3^-$) are the dominant U(VI) species in solution which result in the reduction of the U(VI) removal efficiency.⁴⁴ The maximum removal rate for GC, MGC and GO/Fe₃O₄/GC was 66.30% (pH 6.0), 73.30% (pH 5.0), and 98.70% (pH 5.0), respectively. The sorption efficiency of U(VI) by GO/Fe₃O₄/GC was much higher than that of GC indicating that the addition of GO in the GC molecular enhanced greatly the adsorption property for U(VI). As a consequence, the optimal pH for GC, MGC and GO/Fe₃O₄/GC was selected as 6.0, 5.0 and 5.0 in the next U(VI) adsorption tests, respectively.

The influence of some important co-existing cations (e.g., Na^+ , K^+ , Ca^{2+} , Mg^{2+} , and Al^{3+}) on U(VI) sorption by GO/Fe₃O₄/GC at 298 K and pH 5.0 was shown in Fig. 5B. It was clearly seen that Na^+ , K^+ , Mg^{2+} and Ca^{2+} had no significant competition effects on the sorption of U(VI). In contrast, the presence of Al^{3+} had a suppressive effect on U(VI) sorption. The results showed that the binding ability of cations to U(VI) followed the priority sequence: +3 valence cations (e.g., Al^{3+}) < +2 valence cations (e.g., Mg^{2+} and Ca^{2+}) < +1 valence cations (e.g., Na^+ and K^+) which indicated that the better electrostatic interaction between high valence cations and the adsorbent GO/Fe₃O₄/GC result in the decrease of the adsorption efficiency for U(VI).

Adsorption isotherm. The fit results of Langmuir, Freundlich and Dubinin–Radushkevich (D–R) isotherm models for the U(VI) adsorption on GC and GO/Fe₃O₄/GC are presented in Fig. 6. The Langmuir, Freundlich and D–R isotherm parameters are calculated and listed in Table 1. It was clearly seen that the Langmuir equation of the adsorbents fitted well the experimental data with a higher correlation coefficient compared to Freundlich and D–R adsorption isotherm models. The maximum sorption capacity (Q_m) of U(VI) on GC and GO/Fe₃O₄/GC was determined to be 396.85 mg g⁻¹ and 390.70 mg g⁻¹, respectively, higher than those of the previously reported glucose-based materials (see Table 2), which indicated that GO/Fe₃O₄/GC was a promising adsorbent for the treatment of the uranium-bearing wastewater.

According to the D-R isotherm parameters, the obtained E values reveal the physical or chemical sorption mechanism. According to the literature⁴⁵, if E lies between 8 and 16 kJ mol⁻¹, the sorption process takes place chemically whereas $E < 8$ kJ mol⁻¹ follows the physical sorption. For GC and GO/Fe₃O₄/GC, low E value (< 8 kJ mol⁻¹) obtained in this study suggested that the mechanism of U adsorption was the physical adsorption process due to electrostatic interaction or Van der Waal's attraction.

Table 1. Parameters of Langmuir, Freundlich and D-R model for U(VI) adsorption on GC and GO/Fe₃O₄/GC.

Sorbents	Langmuir			Freundlich			D-R			
	Q_m mg g ⁻¹	k_L L mg ⁻¹	R^2	n	k_F mg ¹⁻ⁿ L ⁿ g ⁻¹	R^2	Q_m mg g ⁻¹	β mol ² (J ²) ⁻¹	E kJ mol ⁻¹	R^2
GC	396.85	0.5796	0.9825	3.20	138.90	0.9322	312.85	0.94	0.73	0.9141
GO/Fe ₃ O ₄ /GC	390.70	0.3420	0.9873	3.49	118.85	0.9275	260.83	0.50	1.00	0.8646

Table 2. Comparison of Q_m of GO/Fe₃O₄/GC with reported other glucose-based sorbents for U(VI) adsorption.

Sorbents	pH	Contact time	m/V (g L ⁻¹)	Q_m (mg g ⁻¹)	References
HTC	6.0	50 min	0.2	62.7	[46]
HCSs-PO ₄ -3	5.0	30 min	0.2	285.70	[47]
HTC-COOH	4.5	22 h	0.5	163	[48]
GC	6.0	24 h	0.15	396.85	This work
GO/Fe ₃ O ₄ /GC	5.0	30 min	0.15	390.70	This work

Adsorption kinetics. Figure 7 presents the time-dependent adsorption rate over contact time ranging from 5 min to 24 h of U(VI) by GC, MGC and GO/Fe₃O₄/GC. As shown in Fig. 7, the adsorption kinetic of GO/Fe₃O₄/GC toward U(VI) indicated a fast adsorption process, and the remove of U(VI) could reach above 98% within 30 min. But the remove of U(VI) by GC could reach 97% after 24 h. Moreover, as presented in Fig. 7 (insert A and B), the correlation coefficients of pseudo second-order model were superior compared to pseudo first-order model which showed that the adsorption of UO₂²⁺ ions onto GO/Fe₃O₄/GC was well fitted by the pseudo-second-order model. Adsorption kinetic parameters of the pseudo first-order and pseudo second-order model for GC, MGC and GO/Fe₃O₄/GC were given in Table 3. The results suggested that the interaction between UO₂²⁺ and the as-prepared adsorbents is controlled by chemical sorption in the rate-controlling steps⁴⁹.

Table 3. Parameters of the pseudo first-order and second-order kinetic models for U adsorption on GC, MGC and GO/Fe₃O₄/GC.

Sorbents	Pseudo first-order model			Pseudo second-order model		
	Q_e (mg g ⁻¹)	k_1 (min ⁻¹)	R^2	Q_e (mg g ⁻¹)	k_2 (g (mg·min) ⁻¹)	R^2
GC	19.3598	0.0930	0.8016	63.82	0.0547	0.9989
MGC	26.2452	0.0098	0.2288	44.50	0.4763	0.9999
GO/Fe ₃ O ₄ /GC	0.7619	0.0788	0.3240	66.36	1.7671	1.0000

Adsorption thermodynamics. The plots of $\ln K_d$ versus $1/T$ onto GC and GO/Fe₃O₄/GC were shown in Fig. 8. The thermodynamic parameters such as enthalpy (ΔH^0), entropy (ΔS^0) and standard free energy (ΔG^0) from 303 K to 333 K in the adsorption processes were calculated according to Eqs. (5) and (6) and given in Table 4. The negative value of ΔH^0 for GC reflected that the adsorption reaction was endothermic. While the positive value of ΔH^0 for GO/Fe₃O₄/GC reflected that the adsorption reaction was exothermic. The positive ΔS^0 and negative ΔG^0 suggested that the spontaneity of the adsorption process.

$$\ln K_d = -\frac{\Delta H^0}{RT} + \frac{\Delta S^0}{R}, \quad (5)$$

$$\Delta G^0 = \Delta H^0 - T\Delta S^0, \quad (6)$$

Table 4. Thermodynamic parameters of U(VI) adsorption on GC and GO/Fe₃O₄/GC.

Sorbents	ΔH^0 (kJ mol ⁻¹)	ΔS^0 (J (mol·K) ⁻¹)	ΔG^0 (kJ mol ⁻¹)			
			303 K	313 K	323 K	333 K
GC	-10.31	0.28	-10.3948	-10.3976	-10.4004	-10.4032
GO/Fe ₃ O ₄ /GC	11.57	65.42	-8.2523	-8.9065	-9.5607	-10.2149

Regenerability of GO/Fe₃O₄/GC. Regeneration is an important aspect in the process of wastewater treatment in view of the cost saving. The reuse of GO/Fe₃O₄/GC was examined in this study. After the adsorption experiments, the obtained U-loaded GO/Fe₃O₄/GC was rinsed and washed with the regenerant (3 M HNO₃) and the deionized water (DW) thoroughly until U(VI) ions were not detected in the rinse solution. Then, the dried and regenerated GO/Fe₃O₄/GC was reused for the further adsorption experiments (the adsorption conditions: pH=5.0, C₀(U)=10 mg L⁻¹, T = 298 K, adsorbent dosage = 0.15 g L⁻¹, and contact time = 24 h). The results proved that GO/Fe₃O₄/GC was used repeatedly for the U(VI) adsorption, and the U(VI) removal rate reached 85.45% after five cycles.

Materials and methods

Materials. Uranyl nitrate ($\text{UO}_2(\text{NO}_3)_2 \cdot 6\text{H}_2\text{O}$) was purchased from Xi'an Dingtian Chemical Reagent Co. (China). The stock solutions of uranium ($5\sim 150 \text{ mg L}^{-1}$) were prepared by dissolving $\text{UO}_2(\text{NO}_3)_2 \cdot 6\text{H}_2\text{O}$ in DW and acidified with a small amount of concentrated HNO_3 . Glucose was obtained from Chengdu Keshi Reagent Co. (China). All reagents were of analytical grade and used without further purification. DW was used throughout the experiments.

Synthesis of glucose-COOH (GC). The hydrothermal carbon (HTC) was synthesized using glucose via a hydrothermal method. Briefly, 6 g of glucose were dissolved in 60 mL DW and placed in a Teflonlined autoclave at 453 K for 24 h. After the autoclave was cooled to room temperature, the solid product HTC was filtered and washed with DW until the filtrate was colorless, and finally dried at 333 K under a vacuum. Finally, carboxyl-rich glucose-COOH (GC) was obtained by heating HTC in a muffle for 5 h at 573 K.

Synthesis of magnetic glucose-COOH (MGC). Firstly, 0.5 g of GC was dissolved in 100 mL DW. Then, 30% $\text{NH}_3 \cdot \text{H}_2\text{O}$ solution was added to the GC solution until the solution pH becomes 11. 1.25 g of $\text{FeSO}_4 \cdot 7\text{H}_2\text{O}$ was added slowly to the mixture under stirring. After stirring for 3 h, the black product (MGC) was collected by magnetic separation, and completely washed with DW and ethanol. Finally, MGC was dried at 323 K in vacuum.

Synthesis of magnetic composite GO/ Fe_3O_4 /GC. Firstly, GO was prepared from natural graphite by the modified Hummers method⁵⁰. In a typical synthesis of GO/ Fe_3O_4 /GC, the mixture of 0.25 g of GO and 0.25 g of GC was dispersed in 100 mL DW under ultrasonic radiation for 3 h. Then, 30% $\text{NH}_3 \cdot \text{H}_2\text{O}$ solution was added to the GO/GC solution until the solution pH becomes 11. 1.25 g of $\text{FeSO}_4 \cdot 7\text{H}_2\text{O}$ was added slowly to the mixture with continuous stirring. After stirring for 3 h, the magnetic black product (GO/ Fe_3O_4 /GC) was collected by magnetic separation, and washed with DW and ethanol. Finally, the product was dried at 323 K in vacuum.

Characterization. The Fourier transform infrared (FTIR) spectra of the as-prepared adsorbents were obtained using a FTIR spectrometer (Bruker VERTEX 70, Germany). The crystal phases of the samples were characterized by X-ray diffraction (XRD) pattern (Dandong 2700 model, China). The morphologies of the products were determined using Scanning Electron Microscope (SEM) (FEI Helios 600i, USA). The magnetic measurements of Fe_3O_4 and GO/ Fe_3O_4 /GC were conducted at 300 K under a varying magnetic field (PPMS-9 ECII, USA Quantum Design Co.). X-ray photoelectron spectrometer (XPS) (Thermo Fisher ESCALAB 250, USA) was used to analyze the chemical composition of the samples. Thermal stability of the products was studied by a thermogravimetric analysis (TGA) system (Netzsch STA449F3, Germany) from 30 to 900 °C at a heating rate of 10 K min⁻¹ under an argon flow.

Adsorption experiments. The influence of pH, co-existing cations, contact time, initial U(VI) concentration, and temperature on the U(VI) removal was investigated. The U(VI) solution pH was adjusted to the desired value using HCl and NaOH. The as-prepared adsorbent was added to 20 mL solution and shaken in a shaker (Kangshi, China). After filtration, the U(VI) concentrations in solutions were determined by an MUA micro-quantity uranium analyzer (Beijing Yulun, China). The removal rate (R , %) and adsorption capacity (Q , mg g⁻¹) were calculated according to Eqs. (7) and (8), respectively.

$$R(\%) = \frac{c_0 - c_t}{c_0} \times 100, \quad (7)$$

$$Q(\text{mg} \cdot \text{g}^{-1}) = \frac{(c_0 - c_t)}{W} \times V, \quad (8)$$

where c_0 (mg L⁻¹) is the initial U(VI) concentration; c_t (mg L⁻¹) is the U(VI) concentration at time t ; V is the volume of the solution (L); W is the dosage of the adsorbent (g).

Conclusions

In summary, three adsorbents GC, MGC and GO/ Fe_3O_4 /GC were facilely prepared using the inexpensive and environmentally benign glucose as a raw material for U(VI) capture via the simple hydrothermal carbonization and magnetization reaction. The optimum adsorption conditions for U(VI) with the initial concentration of 10 mg L⁻¹ was at a pH of 5.0, a dosage of 0.15 g L⁻¹, and contact time of within 30 min when using GO/ Fe_3O_4 /GC as the adsorbent. The existence of co-existing ions in solutions such as Na^+ , K^+ , Mg^{2+} , Ca^{2+} and Al^{3+} had different influence on the removal of uranium by GO/ Fe_3O_4 /GC. Adsorption data of U(VI) by GO/ Fe_3O_4 /GC were in good agreement with Langmuir isotherm

model and pseudo-second-order kinetic model. The composite GO/Fe₃O₄/GC exhibited excellent U(VI) sorption capacities (390.70 mg g⁻¹), and a faster adsorption rate than those of GC, MGC and the previously reported glucose-based materials. The superior U(VI) uptake and fast solid-liquid separation after adsorption were mainly attributed to the abundant presence of GO and magnetic Fe₃O₄ particles in the molecule of GO/Fe₃O₄/GC. The facile production and high stability of GO/Fe₃O₄/GC reinforce its potential in the industrial purification of various pollutants, which paves the way for a new route to develop a novel glucose-based composite as a low-cost and highly efficient adsorbent to remove U(VI) from uranium-containing waste influents. The as-prepared GO/Fe₃O₄/GC has good regenerability which is very important in the practical application.

References

1. Ma, F., Ding, S. L., Ren, H. J. & Liu, Y. H. Sakura-based activated carbon preparation and its performance in supercapacitor applications. *RSC Adv.* **9**, 2474–2483 (2019).
2. Bulusheva, L. G., Sysoev, V. I., Lobiak, E. V., Fedoseeva, Y. V., Makarova, A. A., Dubois, M., Flahaut, E. & Okotrub, A. V. Chlorinated holey double-walled carbon nanotubes for relative humidity sensors. *Carbon* **148**, 413–420 (2019).
3. Xin, B. W. *et al.* Carbon fiber-promoted activation of catalyst for efficient growth of single-walled carbon nanotubes. *Carbon* **156**, 410–415 (2020).
4. Kwon, H. N., Park, G. D., Kang, Y. C. & Roh, K. C. Fabrication of bimodal micro-mesoporous amorphous carbon-graphitic carbon-reduced graphene oxide composite microspheres prepared by pilot-scale spray drying and their application in supercapacitors. *Carbon* **144**, 591–600 (2019).
5. Kim, Y. J., Hong, I., Shim, J. & An, J. C. Preparation and characterization of black liquor-derived activated carbon by self-chemical activation. *Carbon Lett.* **30**, 115–121 (2020).
6. Pi, L. *et al.* Bionic preparation of CeO₂-encapsulated nitrogen self-doped biochars for highly efficient oxygen reduction. *ACS Appl. Mater. Interfaces* **12**, 3642–3653 (2020).
7. Liu, W. J., Li, W. W., Jiang, H. & Yu, H. Q. Fates of chemical elements in biomass during its pyrolysis. *Chem. Rev.* **117**, 6367–6398 (2017).
8. Mitina, A. A., Redkin, A. N. & Yakimov, E. E. New way of the nickel catalyst preparation for carbon nanotubes synthesis by pyrolysis of ethanol vapor. *Fuller. Nanotub. Car. N.* **28(2)**, 112–117 (2020).
9. Wang, J. L. & Wang, S. Z. Preparation, modification and environmental application of biochar: A review. *J. Clean. Prod.* **227**, 1002–1022 (2019).
10. Aftab, F. *et al.* A facile synthesis of FeCo nanoparticles encapsulated in hierarchical N-Doped carbon nanotube/nanofiber hybrids for overall water splitting. *ChemCatChem.* **12**, 932–943 (2020).
11. Tooming, T., Thomberg, T., Kurig, H., Jänes, A. & Lust, E. High power density supercapacitors based on the carbon dioxide activated D-glucose derived carbon electrodes and 1-ethyl-3-methylimidazolium tetrafluoroborate ionic liquid. *J. Power Sources* **280**, 667–677 (2015).
12. Liu, Z. *et al.* New strategy to prepare ultramicroporous carbon by ionic activation for superior CO₂ capture. *Chem. Eng. J.* **337**, 290–299 (2018).
13. Wang, Y. M., Zhou, Y. L., Jiang, G. J., Chen, P. R. & Chen, Z. One-step fabrication of carbonaceous adsorbent from corncob for enhancing adsorption capability of methylene blue removal. *Sci. Rep.* **10**, 12515 (2020).
14. Cai, H. M., Lin, X. Y., Tian, L. Y. & Luo, X. G. One-step hydrothermal synthesis of carbonaceous spheres from glucose with an aluminum chloride catalyst and its adsorption characteristic for uranium(VI). *Ind. Eng. Chem. Res.* **55**, 9648–9656 (2016).
15. Luo, X. W. *et al.* Hydrothermal carbonization of sewage sludge and in-situ preparation of hydrochar/MgAl-layered double hydroxides composites for adsorption of Pb(II). *J. Clean. Prod.* **258**, 120991 (2020).
16. Chen, W. H., Zhang, G. C., Li, D., Ma, S. G., Wang, B. D. & Jiang, X. Preparation of nitrogen-doped porous carbon from waste polyurethane foam by hydrothermal carbonization for H₂S adsorption. *Ind. Eng. Chem. Res.* **59**, 7447–7456 (2020).
17. Wu, J., Yang, J., Huang, G., Xu, C. & Lin, B. Hydrothermal carbonization synthesis of cassava slag biochar with excellent adsorption performance for Rhodamine B. *J. Clean. Prod.* **251**, <https://doi.org/10.1016/j.jclepro.2019.119717>

(2020).

18. Yang, G. Z., Song, S., Li, J., Tang, Z. H., Ye, J. Y. & Yang, J. H. Preparation and CO₂ adsorption properties of porous carbon by hydrothermal carbonization of tree leaves. *J. Mater. Sci. Technol.* **35**, 875–884 (2019).
19. Sheng, K. C. *et al.* Hydrothermal carbonization of cellulose and xylan into hydrochars and application on glucose isomerization. *J. Clean. Prod.* **237**, 117831 (2019).
20. Schonvogel, D. *et al.* Hydrothermal carbonization-derived carbon from waste biomass as renewable Pt support for fuel cell applications: role of carbon activation. *Energy Technol.* **7**, 1900344 (2019).
21. Ning, X. J. *et al.* Physicochemical, structural and combustion properties of hydrochar obtained by hydrothermal carbonization of waste polyvinyl chloride. *Fuel* **270**, 117526 (2020).
22. Sharma, H. B., Sarmah, A. K. & Dubey, B. Hydrothermal carbonization of renewable waste biomass for solid biofuel production: A discussion on process mechanism, the influence of process parameters, environmental performance and fuel properties of hydrochar. *Renew. Sust. Energ. Rev.* **123**, 109761 (2020).
23. Shi, N. *et al.* Formation of soluble furanic and carbocyclic oxy-organics during the hydrothermal carbonization of glucose. *Energy Fuels* **34**, 1830–1840 (2020).
24. Elaigwu, S. E. & Greenway, G. M. Chemical, structural and energy properties of hydrochars from microwave-assisted hydrothermal carbonization of glucose. *Int. J. Ind. Chem.* **7**, 449–456 (2016).
25. Yang, Z. *et al.* Facile synthesis of high-performance nitrogen-doped hierarchically porous carbon for catalytic oxidation. *ACS Sustainable Chem. Eng.* **8**, 4236–4243 (2020).
26. Jaramillo, D. E. *et al.* Selective nitrogen adsorption via backbonding in a metal-organic framework with exposed vanadium sites. *Nature Mater.* **19**, 517–521 (2020).
27. Gupta, K. M., Zhang, K. & Jiang, J. W. Glucose recovery from aqueous solutions by adsorption in metal-organic framework MIL-101: a molecular simulation study. *Sci. Rep.* **5**, 12821 (2015).
28. Wang, B., Xu, X. Y., Tang, H., Mao, Y. L., Chen, H. H. & Ji, F. Y. Highly efficient adsorption of three antibiotics from aqueous solutions using glucose-based mesoporous carbon. *Appl. Surf. Sci.* **528**, 147048 (2020).
29. Li, K. R., Zhou, M. H., Liang, L., Jiang, L. L. & Wang, W. Ultrahigh-surface-area activated carbon aerogels derived from glucose for high-performance organic pollutants adsorption. *J. Colloid Interf. Sci.* **546**, 333–343 (2019).
30. Yue, L. M. *et al.* Efficient CO₂ adsorption on nitrogen-doped porous carbons derived from D-glucose. *Energy Fuels* **32**, 6955–6963 (2018).
31. Meng, L. *et al.* Surface carboxyl-activated polyester (PET) fibers decorated with glucose carbon microspheres and their enhanced selective adsorption for dyes. *J. Phys. Chem. Solids* **123**(1), 378–388 (2018).
32. Cai, H. M., Lin, X. Y., Qin, Y. & Luo, X. G. Hydrothermal synthesis of carbon microsphere from glucose at low temperature and its adsorption property of uranium(VI). *J. Radioanal. Nucl. Chem.* **311**, 695–706 (2017).
33. Wang, G. F., Wang, S., Sun, W., Sun, Z. M. & Zheng, S. L. Synthesis of a novel illite@carbon nanocomposite adsorbent for removal of Cr(VI) from wastewater. *J. Environ. Sci.* **57**, 62–71 (2017).
34. Jiang, X. Q., Ruan, G. H., Huang, Y. P., Chen, Z. Y., Yuan, H. M. & Du, F. Y. Assembly and application advancement of organic-functionalized graphene-based materials: A review. *J. Sep. Sci.* **43**, 1544–1557 (2020).
35. Ahmad, S. Z. N., Salleh, W. N. W., Ismail, A. F., Yusof, N., Yusop, M. Z. M. & Aziz, F. Adsorptive removal of heavy metal ions using graphene-based nanomaterials: Toxicity, roles of functional groups and mechanisms. *Chemosphere* **248**, 126008 (2020).
36. Smith, A. T., Marie, A., Zeng, S., Liu, B. & Sun, L. Synthesis, properties, and applications of graphene oxide/reduced graphene oxide and their nanocomposites. *Nano Mater. Sci.* **1**, 31–47 (2019).
37. Xie, A. T. *et al.* Novel graphene oxide–confined nanospace directed synthesis of glucose-based porous carbon nanosheets with enhanced adsorption performance. *ACS Sustainable Chem. Eng.* **5**, 11566–11576 (2017).
38. Martín-Jimeno, F. J., Suárez-García, F., Paredes, J. I., Martínez-Alonso, A. & Tascón, J. M. D. Activated carbon xerogels with a cellular morphology derived from hydrothermally carbonized glucose-graphene oxide hybrids and their performance towards CO₂ and dye adsorption. *Carbon* **81**, 137–147 (2015).
39. Yu, J. *et al.* Hollow FeP/Fe₃O₄ hybrid nanoparticles on carbon nanotubes as efficient electrocatalysts for the oxygen evolution reaction. *ACS Appl. Mater. Interfaces* **12**, 12783–12792 (2020).
40. Pan, J. L. *et al.* Shape anisotropic Fe₃O₄ nanotubes for efficient microwave absorption. *Nano Res.* **13**(3), 621–629

(2020).

41. Boruah, P. K., Borah, D. J., Handique, J., Sharma, P., Sengupta, P. & Das, M. R. Facile synthesis and characterization of Fe₃O₄ nanopowder and Fe₃O₄/reduced graphene oxide nanocomposite for methyl blue adsorption: A comparative study. *J. Environ. Chem. Eng.* **3(3)**, 1974–1985 (2015).
42. Cai, H. M., Lin, X. Y., Qin, Y. & Luo, X. G. Hydrothermal synthesis of carbon microsphere from glucose at low temperature and its adsorption property of uranium(VI). *J. Radioanal. Nucl. Chem.* **311**, 695–706 (2017).
43. Liu, T. & Xu, Y. B. Synthesis of nanocrystalline LaFeO₃ powders via glucose sol-gel route. *Mater. Chem. Phys.* **129**, 1047–1050 (2011).
44. Liu, X. H. *et al.* Polyaniline (PANI) modified bentonite by plasma technique for U(VI) removal from aqueous solution. *Appl. Surf. Sci.* **411**, 331–337 (2017).
45. Liu, R., Zhang, W., Chen, Y. T. & Wang, Y. S. Uranium (VI) adsorption by copper and copper/iron bimetallic central MOFs. *Colloid. Surface. A.* **587**, DOI: 10.1016/j.colsurfa.2019.124334 (2020).
46. Zhang, Z. B., Cao, X. H., Liang, P. & Liu, Y. H. Adsorption of uranium from aqueous solution using biochar produced by hydrothermal carbonization. *J. Radioanal. Nucl. Chem.* **295**, 1201–1208 (2013).
47. Zhang, Z. B., Zho, Z. W., Cao, X. H., Liu, Y. H., Xiong, G. X. & Liang, P. Removal of uranium(VI) from aqueous solutions by new phosphorus-containing carbon spheres synthesized via one-step hydrothermal carbonization of glucose in the presence of phosphoric acid. *J. Radioanal. Nucl. Chem.* **299**, 1479–1487 (2014).
48. Cai, H. M., Lin, X. Y., Qin, Y. & Luo, X. G. Hydrothermal synthesis of carbon microsphere from glucose at low temperature and its adsorption property of uranium(VI). *J. Radioanal. Nucl. Chem.* **311**, 695–706 (2017).
49. Vu, H. C., Dwivedi, A. D., Le, T. T. Seo, S. H., Kim, E. J. & Chang, Y. S. Magnetite graphene oxide encapsulated in alginate beads for enhanced adsorption of Cr(VI) and As(V) from aqueous solutions: Role of crosslinking metal cations in pH control. *Chem. Eng. J.* **307(Complete)**, 220–229 (2017).
50. Ma, J., Liu, C. H., Li, R. & Wang, J. Properties and structural characterization of oxide starch/chitosan/graphene oxide biodegradable nanocomposites. *J. Appl. Polym. Sci.* **123(5)**, 2933–2944 (2012).

Acknowledgements

This work is financially supported by the National Natural Science Foundation of China (21407132). We also gratefully acknowledge Jingrong Zhong, Qifa Pan, Yi Liu, Ce Ma and Bingqing Li for the characterizations of the samples.

Author contributions

Aili Yang designed and performed all the experiments, analyzed the results, and wrote the manuscript. Zhijun Wang and Yukuan Zhu carried out the adsorption experiments.

Competing interests

The authors declare no competing interests.

Figure caption list

Figure 1. The fabrication process and magnetization curve of GO/Fe₃O₄/GC.

Figure 2. IR spectra (A), XRD patterns (B) and TGA curves (C) of the samples.

Figure 3. XPS survey spectra of Fe₃O₄, glucose, GC, MGC and GO/Fe₃O₄/GC (A) and the high-resolution Fe 2p spectra of Fe₃O₄ and GO/Fe₃O₄/GC (B).

Figure 4. Schematic diagram of a possible formation mechanism of GO/Fe₃O₄/GC.

Figure 5. Effect of pH (A) and co-existing ions (B) on the U(VI) adsorption. $C_{(U)initial} = 10 \text{ mg L}^{-1}$, $C_{sorberent} = 0.25 \text{ g L}^{-1}$, $C_{co-existing \text{ ions}} = 2.5 \text{ g L}^{-1}$, and contact time = 30 min.

Figure 6. The fit results of Langmuir and Freundlich (A) and D-R (B) isotherm models for GC and GO/Fe₃O₄/GC. pH =

5.0 and 6.0, $C_{(U)initial} = 5\sim 150 \text{ mg L}^{-1}$, $C_{sorbent} = 0.15 \text{ g L}^{-1}$, and contact time = 24 h.

Figure 7. Influence of contact time on U(VI) sorption by GC, MGC and GO/Fe₃O₄/GC. Insert A and B are linear fit of the pseudo first-order and pseudo second-order kinetics models, respectively. pH = 5.0 and 6.0, $C_{(U)initial} = 10 \text{ mg L}^{-1}$, and $C_{adsorbent} = 0.15 \text{ g L}^{-1}$.

Figure 8. Plots of $\ln K_d$ versus $1/T$ for U(VI) adsorption onto GC and GO/Fe₃O₄/GC. pH = 5.0 and 6.0, $C_{(U)initial} = 10 \text{ mg L}^{-1}$, $C_{sorbent} = 0.15 \text{ g L}^{-1}$, $T = 303 \text{ K}$, 313 K , 323 K and 333 K , and contact time = 24 h.

Figures

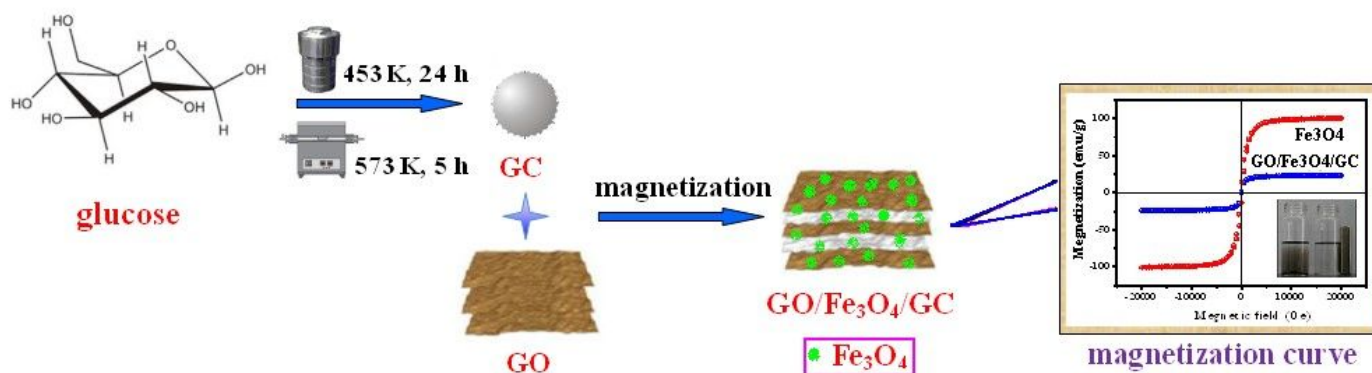


Figure 1

The fabrication process and magnetization curve of GO/Fe₃O₄/GC

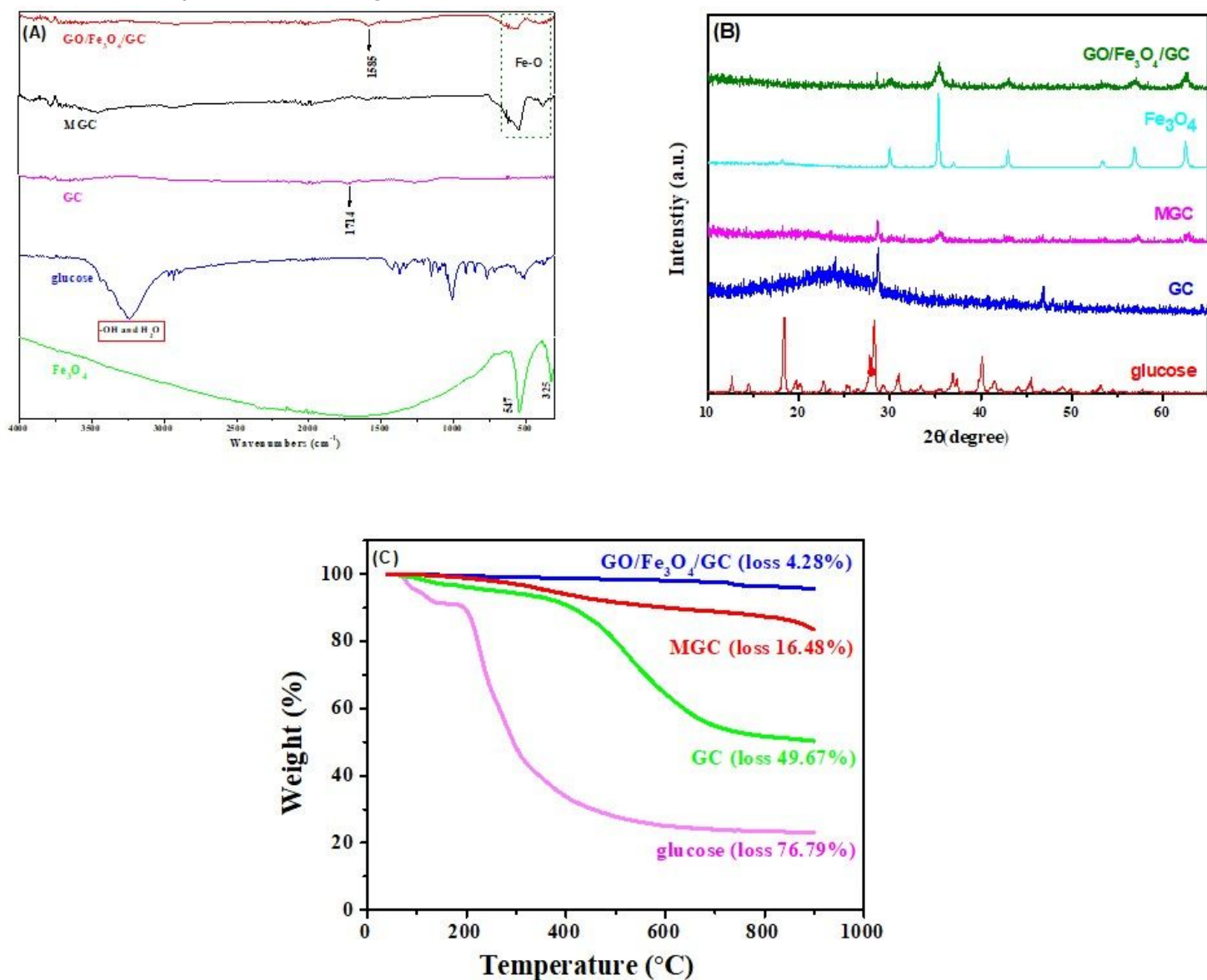


Figure 2

IR spectra (A), XRD patterns (B) and TGA curves (C) of the samples.

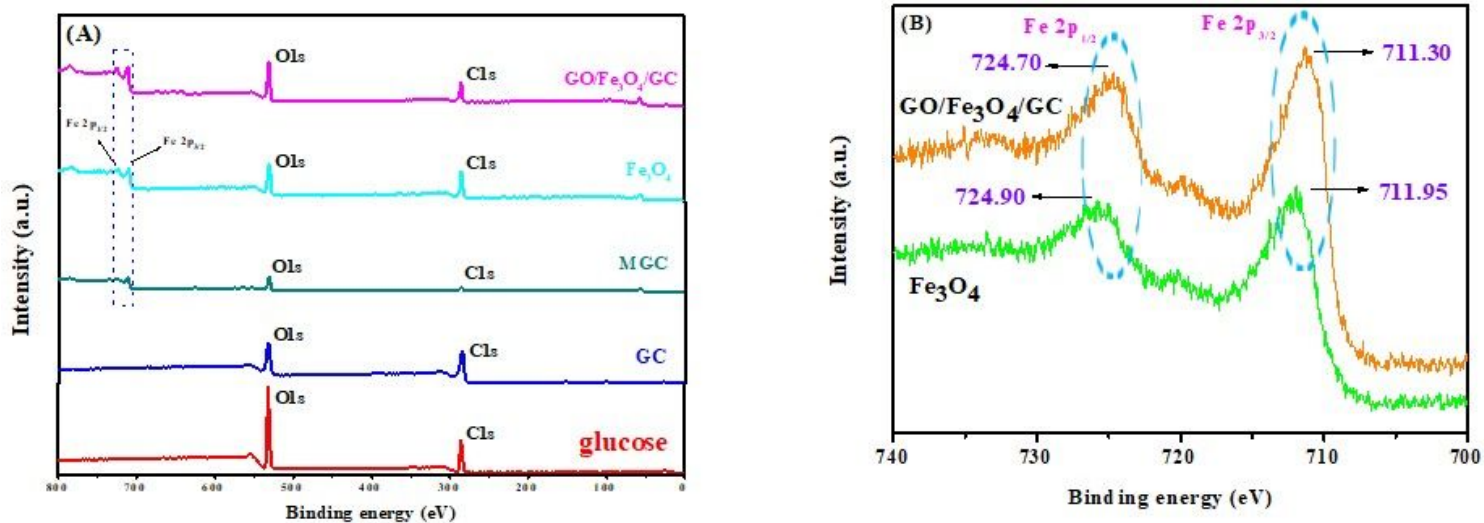


Figure 3

XPS survey spectra of Fe_3O_4 , glucose, GC, MGC and $GO/Fe_3O_4/GC$ (A) and the high-resolution Fe 2p spectra of Fe_3O_4 and $GO/Fe_3O_4/GC$ (B).

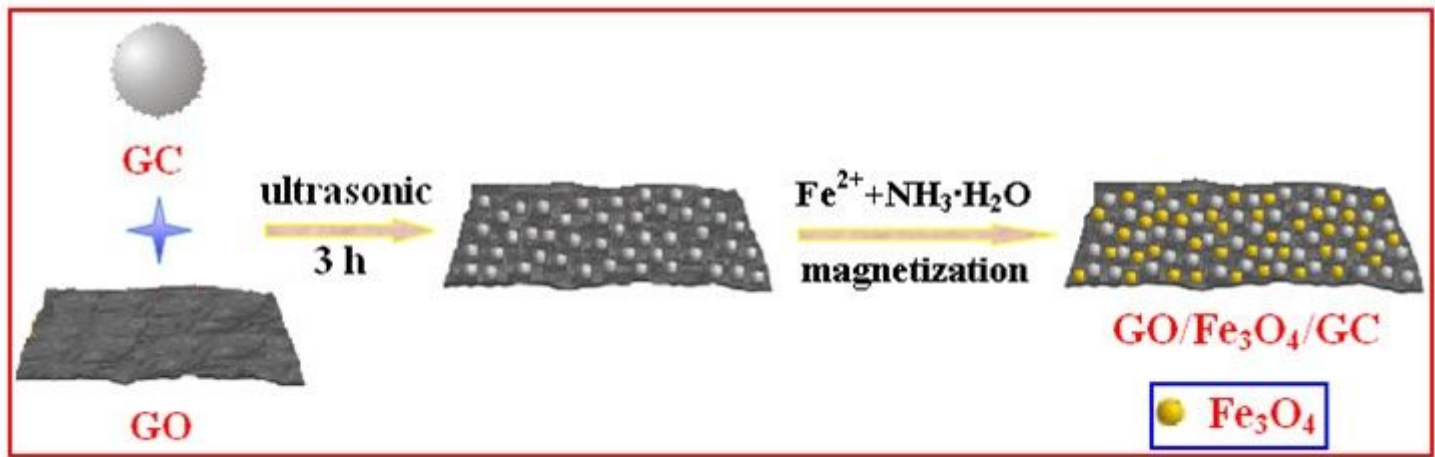


Figure 4

Schematic diagram of a possible formation mechanism of $GO/Fe_3O_4/GC$.

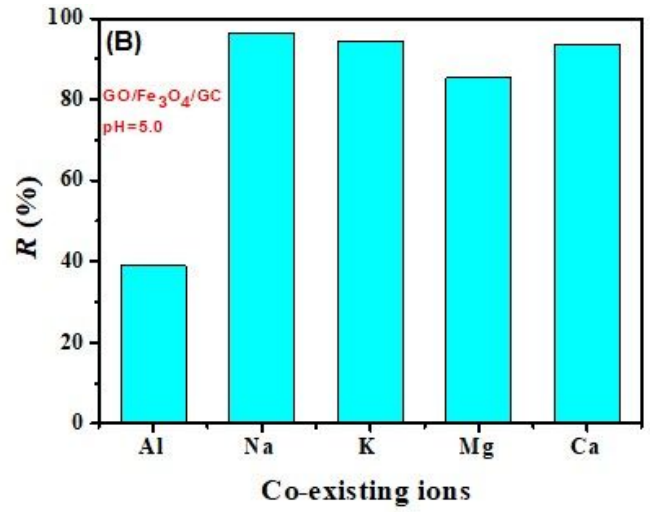
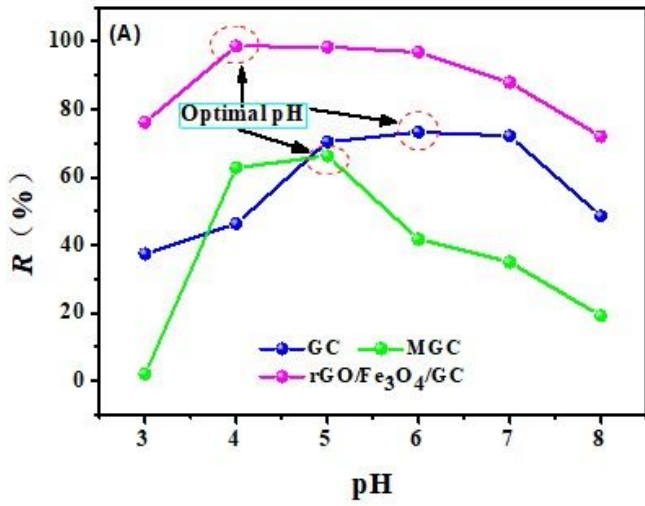


Figure 5

Effect of pH (A) and co-existing ions (B) on the U(VI) adsorption. $C(U)_{\text{initial}} = 10 \text{ mg L}^{-1}$, $C_{\text{adsorbent}} = 0.25 \text{ g L}^{-1}$, $C_{\text{co-existing ions}} = 2.5 \text{ g L}^{-1}$, and contact time = 30 min.

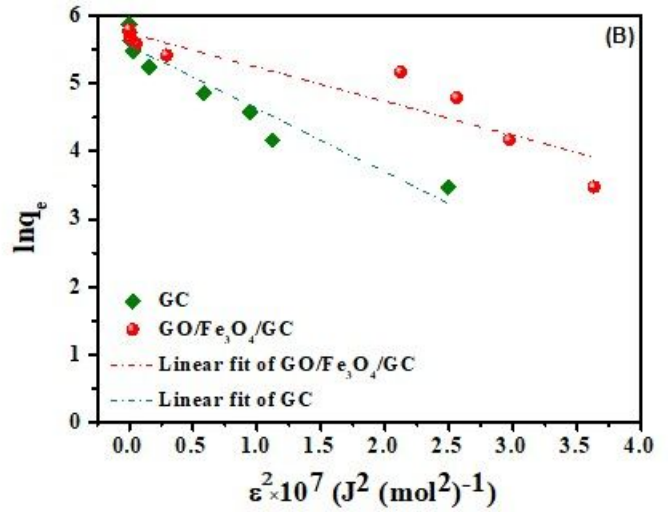
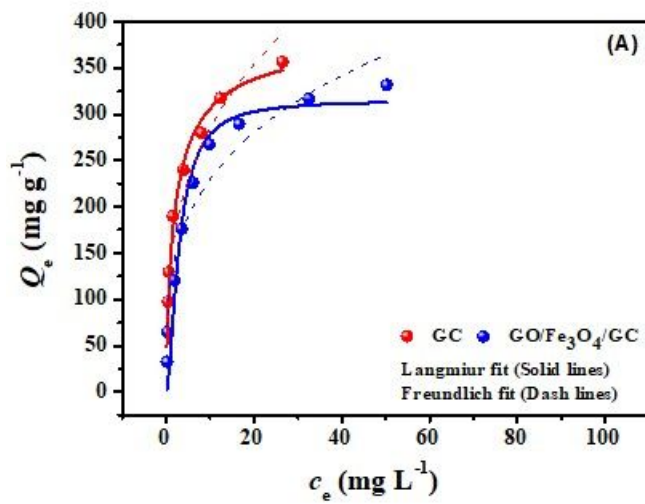


Figure 6

The fit results of Langmuir and Freundlich (A) and D-R (B) isotherm models for GC and GO/Fe₃O₄/GC. pH = 5.0 and 6.0, $C(U)_{\text{initial}} = 5 \sim 150 \text{ mg L}^{-1}$, $C_{\text{adsorbent}} = 0.15 \text{ g L}^{-1}$, and contact time = 24 h.

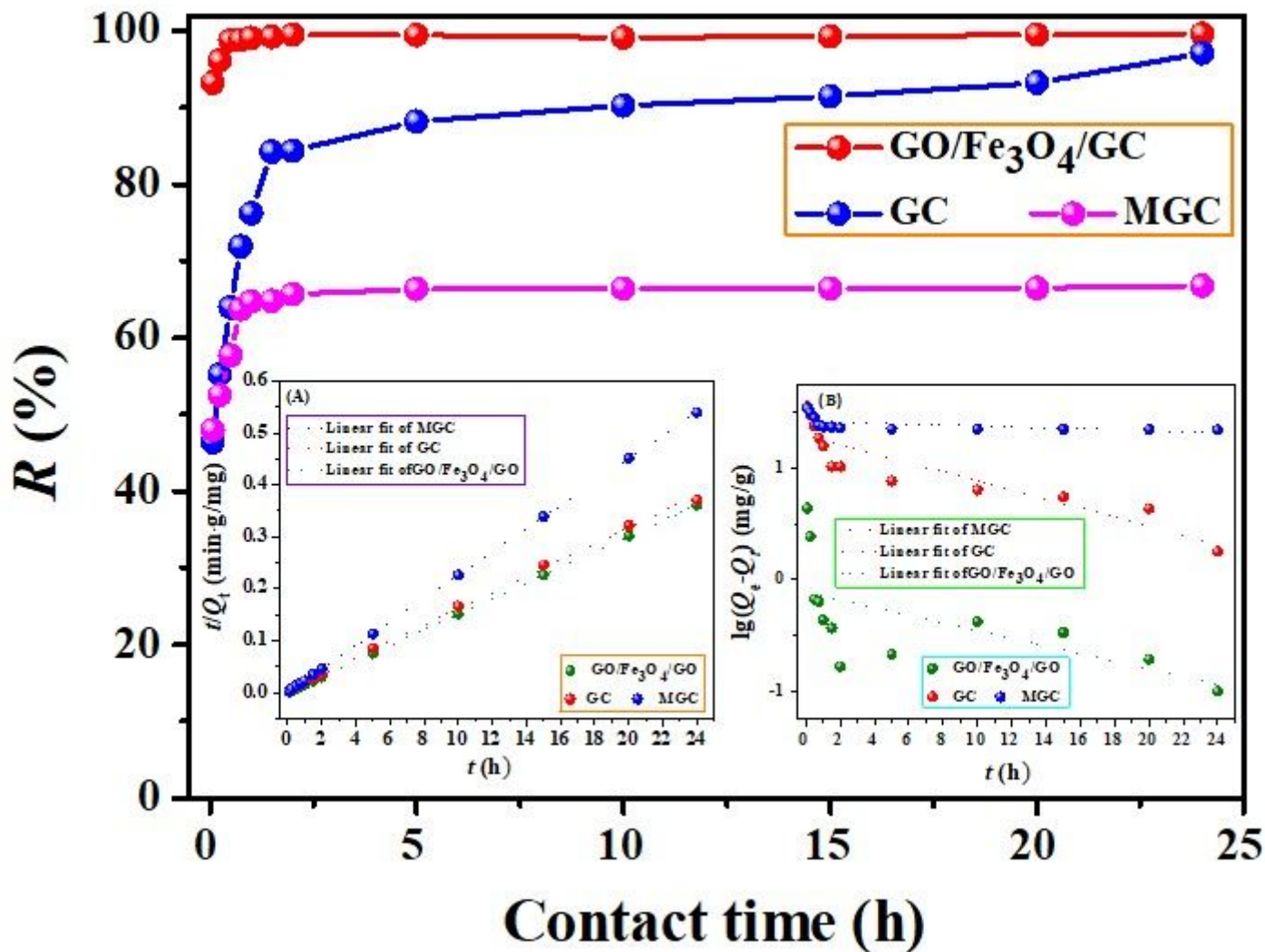


Figure 7

Influence of contact time on U(VI) sorption by GC, MGC and GO/Fe₃O₄/GC. Insert A and B are linear fit of the pseudo first-order and pseudo second-order kinetics models, respectively. pH = 5.0 and 6.0, C(U)_{initial} = 10 mg L⁻¹, and C_{adsorbent} = 0.15 g L⁻¹.

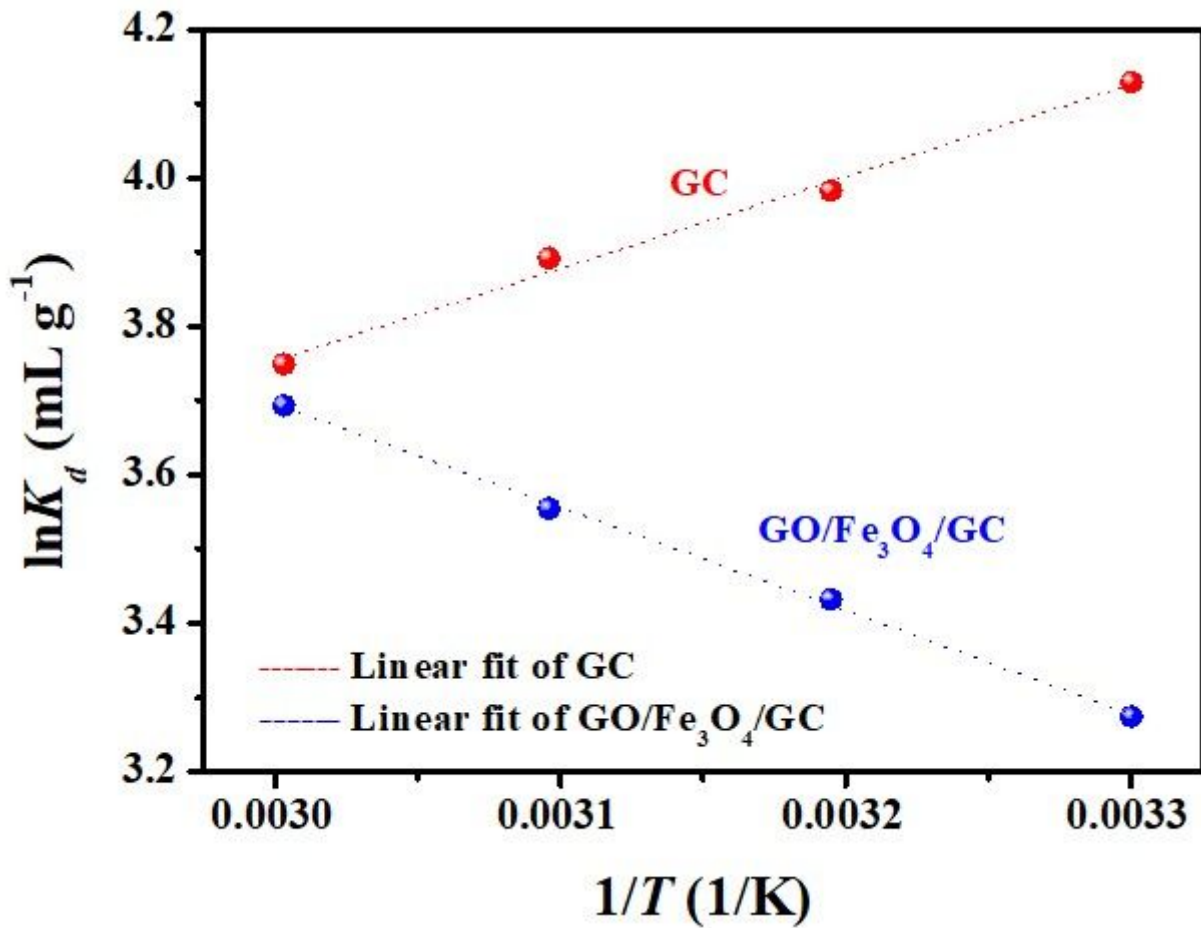


Figure 8

Plots of $\ln K_d$ versus $1/T$ for U(VI) adsorption onto GC and GO/Fe₃O₄/GC. pH = 5.0 and 6.0, $C(U)_{initial} = 10 \text{ mg L}^{-1}$, $C_{sorbent} = 0.15 \text{ g L}^{-1}$, $T = 303 \text{ K}, 313 \text{ K}, 323 \text{ K}$ and 333 K , and contact time = 24 h.